Electronic Supplementary Material (ESI) for Nanoscale.

Supporting Information

to

Switchable Dissociation of Excitons bound at Strained CdTe/CdS Interfaces

Florian Enders,[†] Arne Budweg,[‡] Peng Zeng,[¶,‖] Jannika Lauth,[§,⊥] Trevor A. Smith,[¶] Daniele Brida,[‡,#] and Klaus Boldt[*,†]

†*Department of Chemistry, University of Konstanz, 78457 Konstanz, Germany*

‡*Department of Physics, University of Konstanz, 78457 Konstanz, Germany*

¶*School of Chemistry, The University of Melbourne, Parkville, Victoria 3010, Australia*

§*Department of Chemical Engineering, Delft University of Technology, Van der Maasweg 9, NL-2629 HZ Delft, The Netherlands*

‖*Present address: School of Materials and Energy & Center for Applied Chemistry, University of Electronic Science and Technology of China, Chengdu 611731, P.R. China*

⊥*Institute for Chemistry, Carl von Ossietzky University, Carl-von-Ossietzky-Str. 9-11, 26129 Oldenburg*

#*Faculty of Science, Technology and Communication, University of Luxembourg, 162 A, Avenue de la Faïencerie, L-1511 Luxembourg*

E-mail: klaus.boldt@uni-konstanz.de

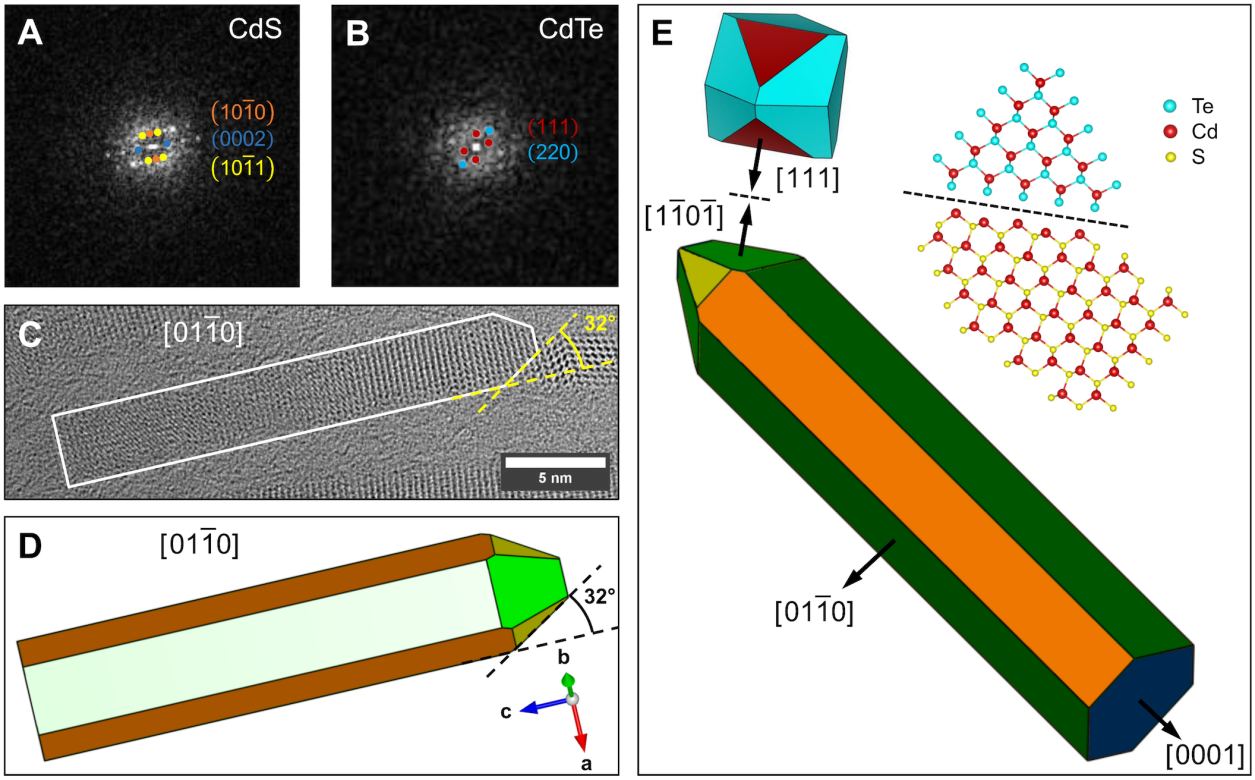

Figure S1: FFTs from hexagonal CdS (A) and cubic CdTe (B) regions of the CdTe@CdSe/CdS nanorods with the reflexes and corresponding lattice planes indicated by color. (C) High-resolution and Cs-corrected TEM micrograph and (D) cartoon representation of a tipped nanorod. The axis perpendicular to the image is [01$\bar{1}$0] and the angle between the lattice planes at the CdTe/CdS interface is indicated with respect to the wurtzite *c*-axis. (E) Schematic of how CdS and CdTe are attached *via* a {10$\bar{1}\bar{1}$} and {111} facet, respectively. The ball-and-stick model illustrates the lattice mismatch between CdS and CdTe.

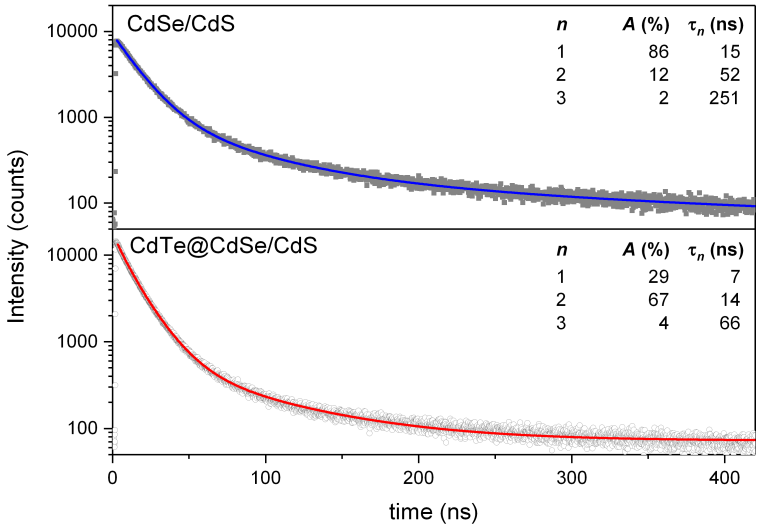

Figure S2: PL decay of CdSe/CdS (top) and CdTe@CdSe/CdS (bottom) for nanorods with 2.9 nm needs. The data were fit to a triple exponential decay function.

Table S1: Lattice parameters, dielectric constants for the static (ϵ_0) and optic (ϵ_∞) limit, elastic stiffness constant C_{ij}, band gap E_g, valence band offset E_{VB} relative to ZnS, effective masses with respect to the [0001] crystal axis in units of the electron rest mass, spin-orbit Δ_{so} and crystal field Δ_{cr} splitting. a_0^Γ and $D_{1\text{-}6}$ are deformation potentials of the conduction and valence band, respectively. Parameters are given perpendicular and parallel to the c-axis of the wurtzite structure; electron effective mass and the deformation potentials are used within cubic approximation. All parameters were taken from [1], except relative band offsets, which were taken from [2]. Values for CdTe were calculated from the zincblende values.

	CdSe	**CdS**	**CdTe**	**Unit**
a	4.297	4.146	4.58	Å
c	7.02	6.713	7.52	Å
$\epsilon_{0,\perp}$	9.29	8.28	10.4	
$\epsilon_{0,\parallel}$	10.16	8.73	10.4	
$\epsilon_{\infty,\perp}$	6.20	5.23	7.1	
$\epsilon_{\infty,\parallel}$	6.30	5.29	7.1	
C_{11}	7.41	8.65	53.5	GPa
C_{12}	4.52	5.40	36.9	GPa
C_{13}	3.9	4.73	36.9	GPa
C_{33}	8.43	9.44	53.5	GPa
C_{44}	1.34	1.50	20.2	GPa
E_g	1.846	2.58	1.60	eV
E_{VB}	0.6	0.18	1.17	eV
m^*_{e}	0.112	0.21	0.090	m_0
$m^*_{\mathrm{hh},\parallel}$	0.58	0.43	0.82	m_0
$m^*_{\mathrm{hh},\perp}$	1.79	1.96	0.82	m_0
$m^*_{\mathrm{lh},\parallel}$	1.09	0.70	0.145	m_0
$m^*_{\mathrm{lh},\perp}$	0.3	0.43	0.145	m_0
$m^*_{\mathrm{so},\parallel}$	0.81	0.79	0.24	m_0
$m^*_{\mathrm{so},\perp}$	0.44	0.37	0.24	m_0
Δ_{so}	0.42	0.070	0.900	eV
Δ_{cr}	0.039	0.026	0.0465	eV
a_0^Γ	-2.3	-2.9	-2.9	eV
D_1	-14.0	-4.16	-4.53	eV
D_2	-6.36	3.46	3.09	eV
D_3	7.62	7.62	7.62	eV
D_4	-3.81	-3.81	-3.81	eV
D_5	-2.94	-4.89	-3.04	eV
D_6	-2.93	-8.44	-3.21	eV

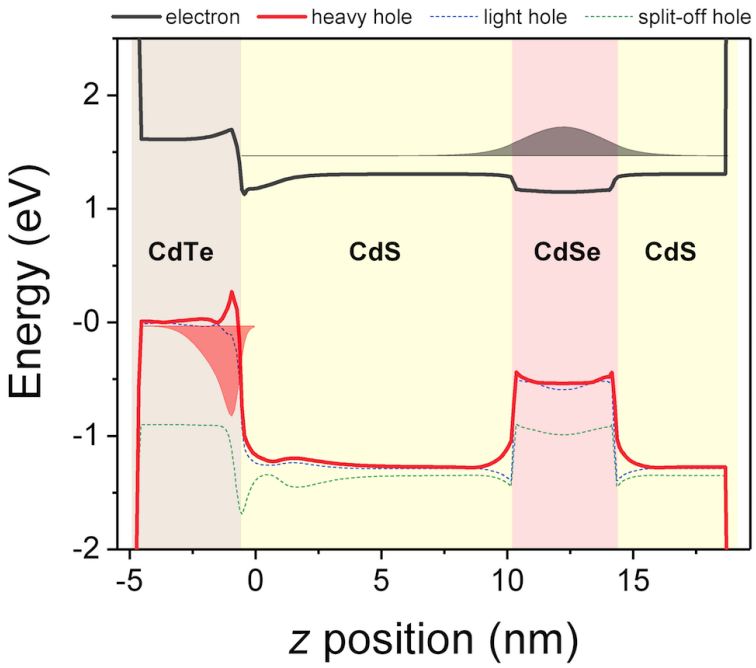

Figure S3: Calculated band structure of a CdTe@CdSe/CdS tipped nanorod with a 4.0 nm CdSe seed, and hexagonal cross section along the wurtzite [0001] axis. Band edges of the conduction band and three valence bands are shown, as well as the lowest energy level and wave function for electron (black) and hole (red). Compared to Figure 2A from the main text one can observe a lower energy of the first electron and hole state, caused by the smaller size quantization perpendicular to the *c*-axis.

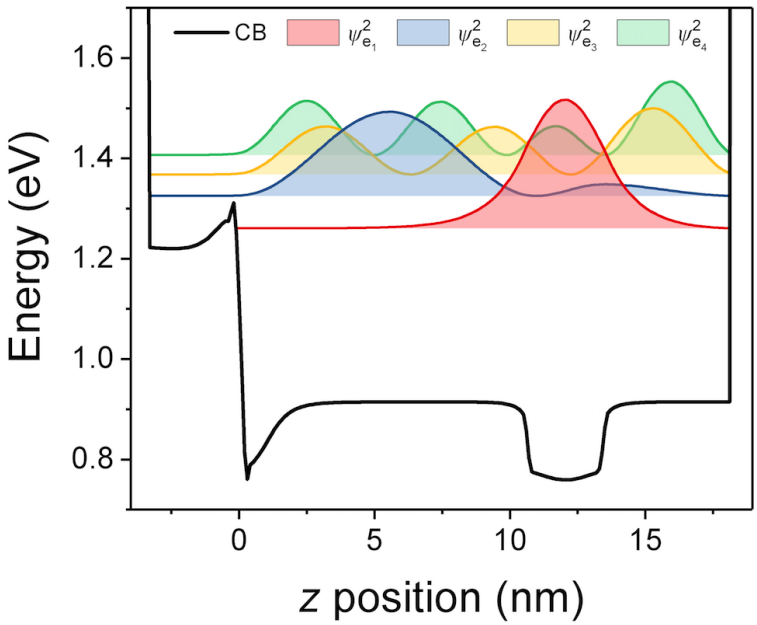

Figure S4: Calculated probability densities $|\psi|^2$ of the first four electron states in the conduction band of CdTe@CdSe/CdS nanorods based on 2.9 nm CdSe seeds. All states have negligible probability density in the CdTe tip.

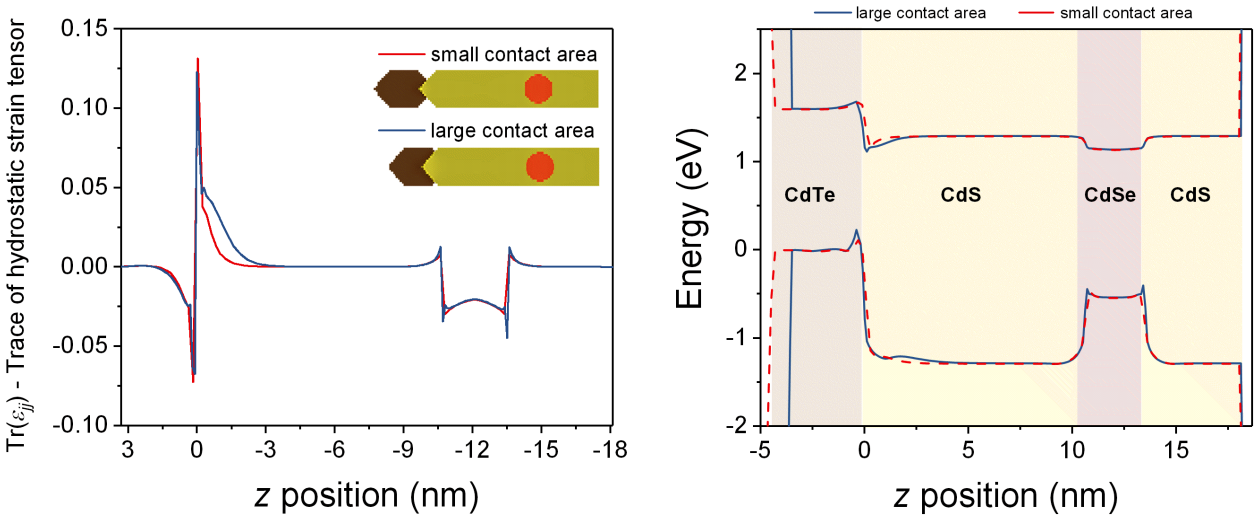

Figure S5: Calculated hydrostatic strain (left) and band structure of the conduction and heavy hole valence band (right) for two different contact areas between CdTe and CdS. With increasing contact area the hydrostatic strain increases in the tip of the CdS rod.

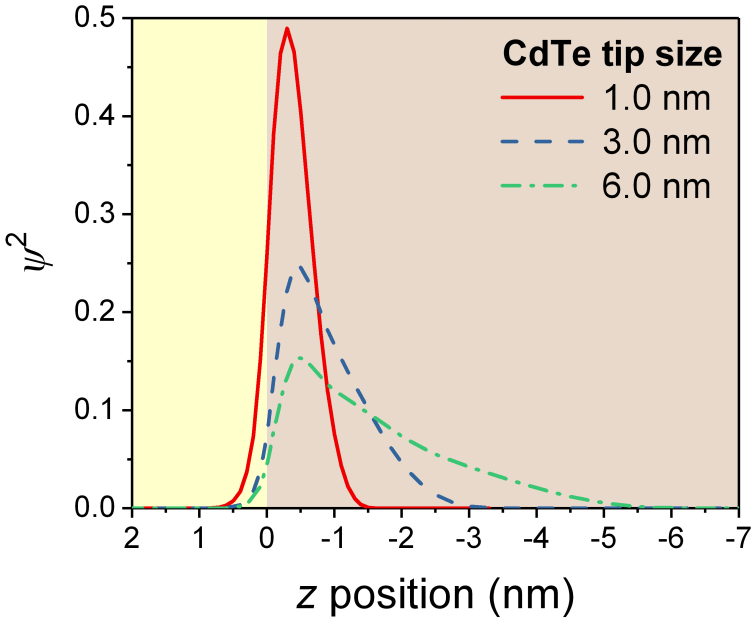

Figure S6: Calculated probability density $|\psi|^2$ of the hole at the CdTe/CdS interface as a function of CdTe tip size. The size of the tip was varies between 1 and 6 nm in direction of the *c*-axis. While a larger tip delocalized the hole to some extent the highest probability density is found close to the interface.

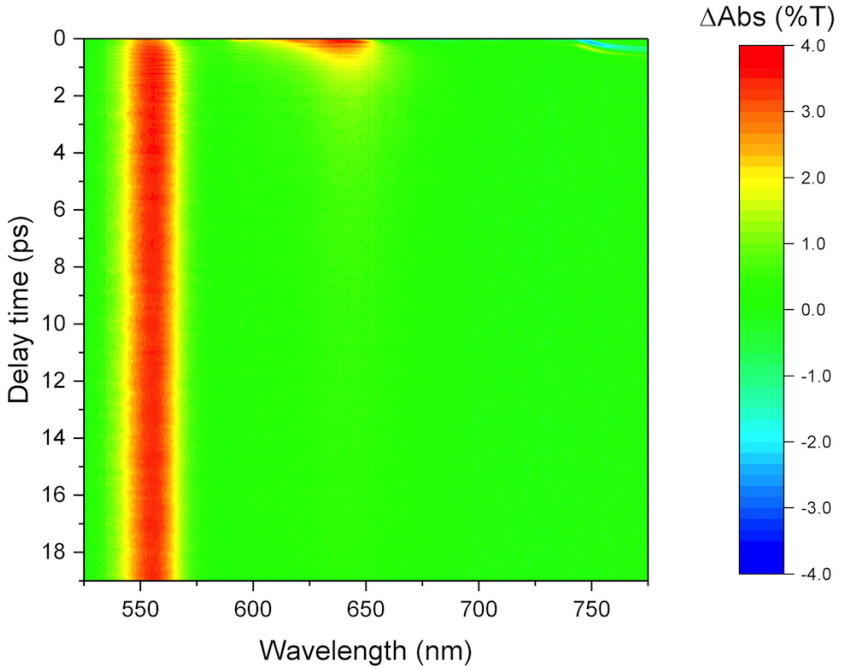

Figure S7: 2D plot of the chirped TA spectrum of CdTe@CdSe/CdS nanorods with a 2.9 nm CdSe seed after pumping at 540 nm. A noticable chirp can be seen at wavelengths > 730 nm only, where no signal is found.

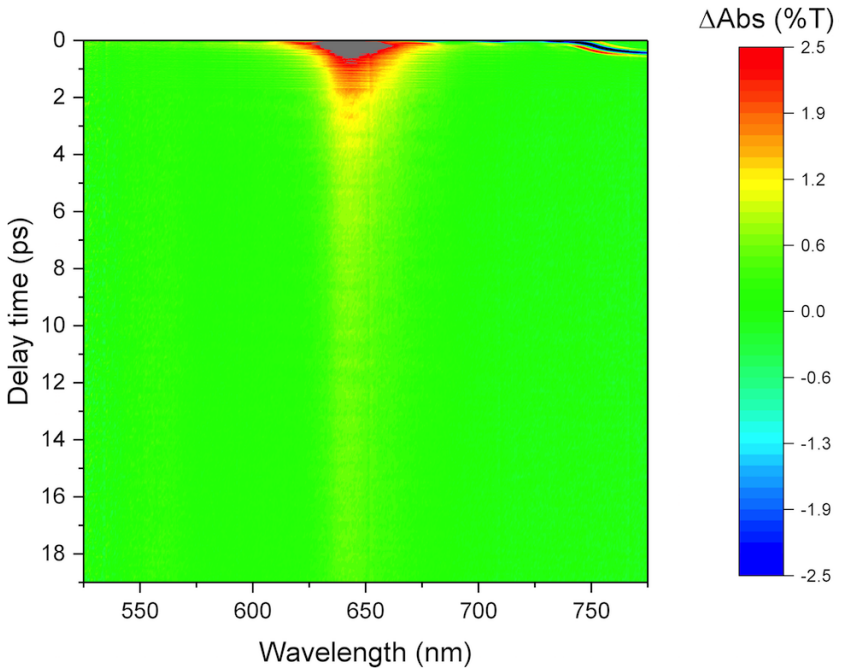

Figure S8: 2D plot of the chirped TA spectrum of CdTe@CdSe/CdS nanorods with a 2.9 nm CdSe seed after pumping at 640 nm.

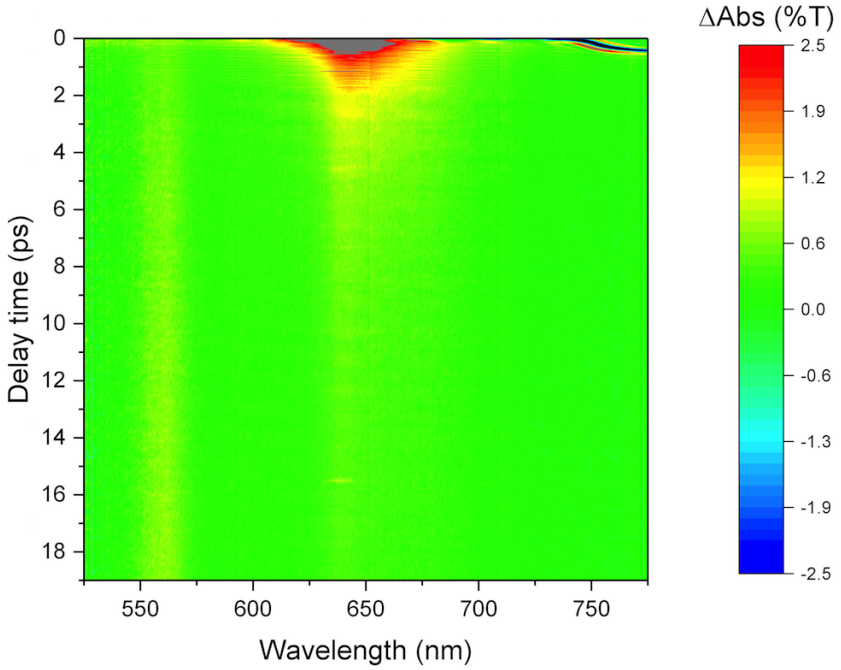

Figure S9: 2D plot of the chirped TA spectrum of CdTe@CdSe/CdS nanorods with a 2.9 nm CdSe seed in the presence pf 4-MPA after pumping at 640 nm.

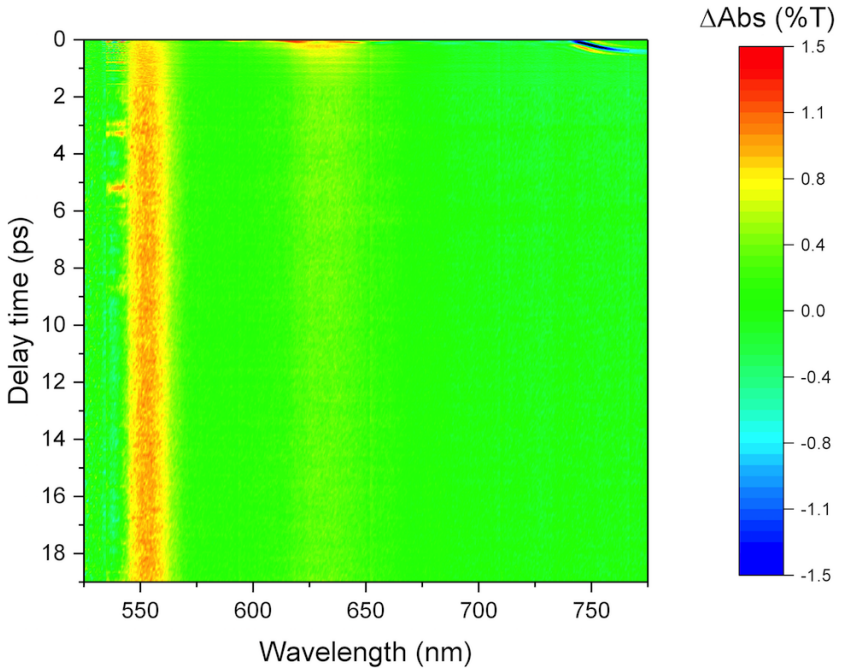

Figure S10: 2D plot of the chirped TA spectrum of CdTe@CdSe/CdS nanorods with a 2.9 nm CdSe seed after ligand exchange to thioglycolic acid and transfer to deaerated water. The sample was pumped at 540 nm.

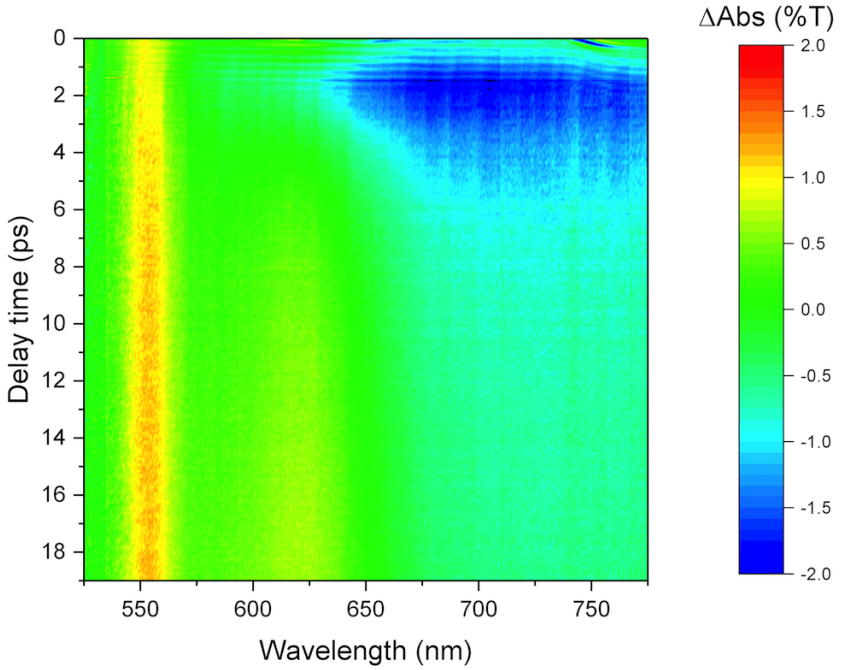

Figure S11: 2D plot of the chirped TA spectrum of CdTe@CdSe/CdS nanorods with a 2.9 nm CdSe seed after ligand exchange to thioglycolic acid and transfer to air-saturated water. The sample was pumped at 540 nm.

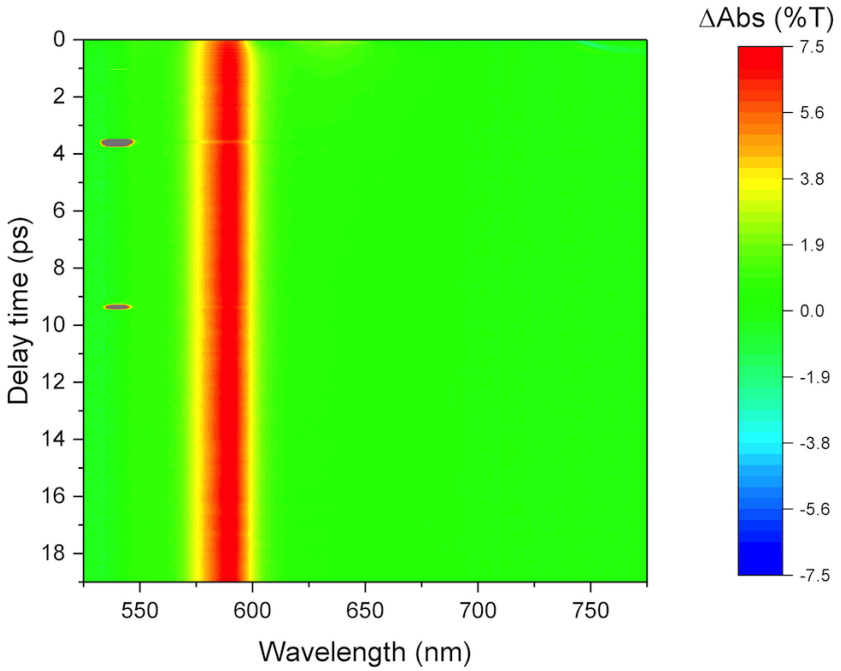

Figure S12: 2D plot of the chirped TA spectrum of CdTe@CdSe/CdS nanorods with a 4.0 nm CdSe seed after pumping at 540 nm.

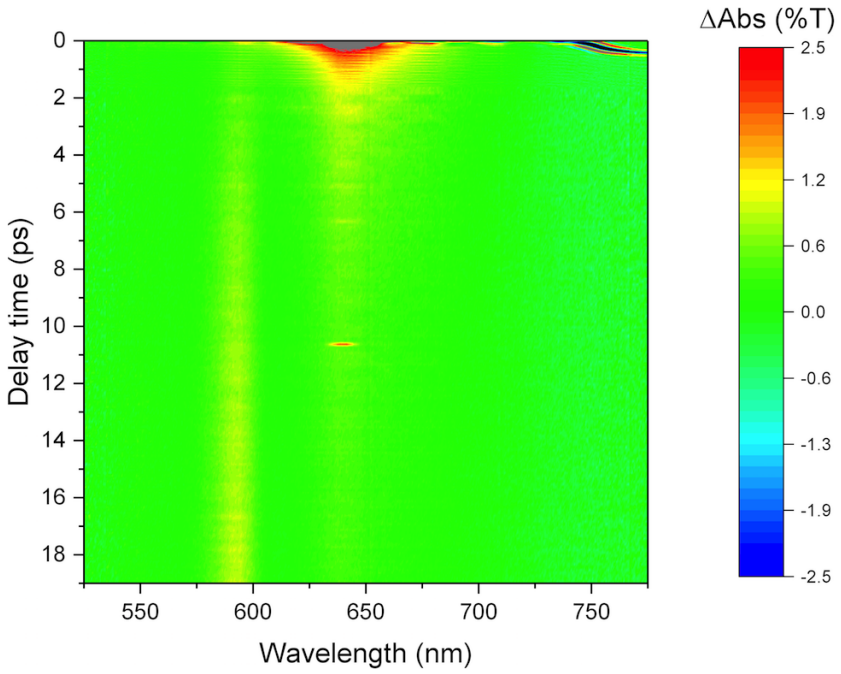

Figure S13: 2D plot of the chirped TA spectrum of CdTe@CdSe/CdS nanorods with a 4.0 nm CdSe seed after pumping at 640 nm.

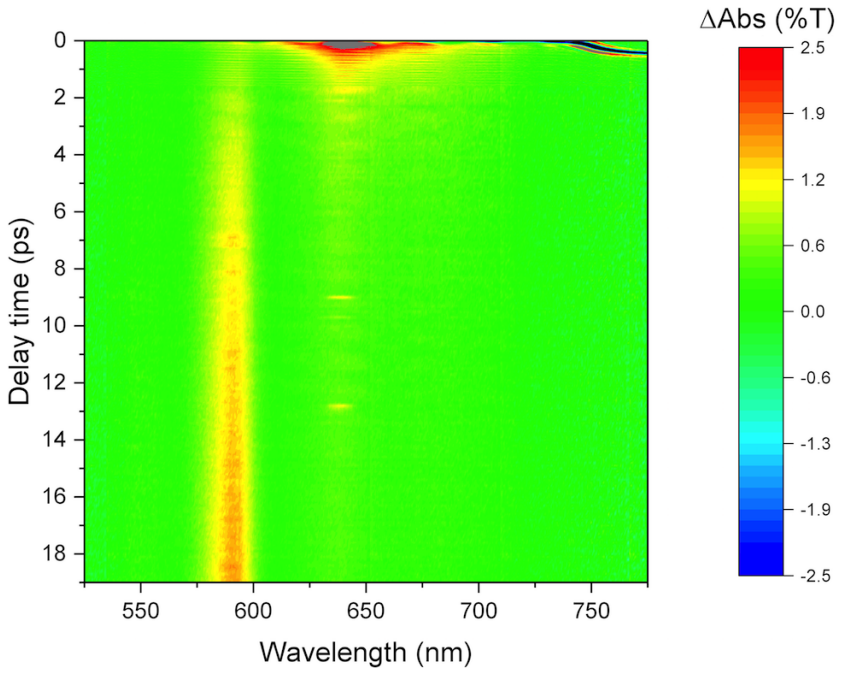

Figure S14: 2D plot of the chirped TA spectrum of CdTe@CdSe/CdS nanorods with a 4.0 nm CdSe seed in the presence pf 4-MPA after pumping at 640 nm.

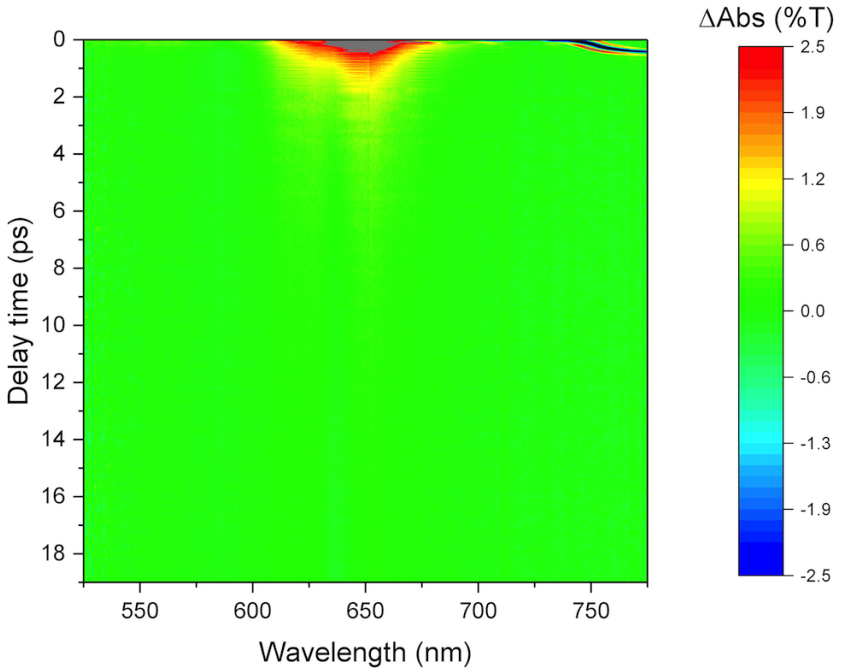

Figure S15: 2D plot of the chirped TA spectrum of pure CdTe nanocrystals with a diameter of 4.5 nm, after pumping at 640 nm.

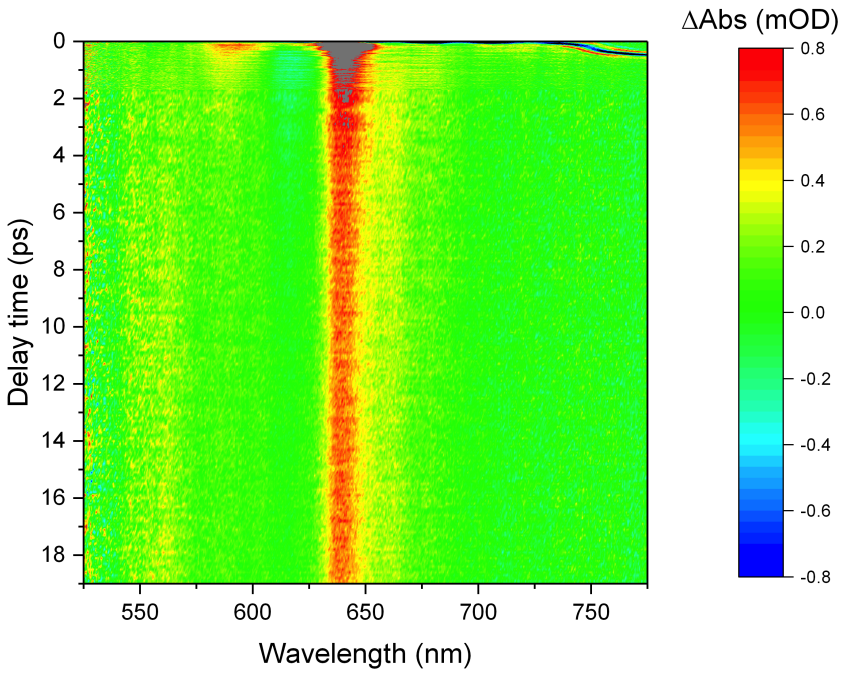

Figure S16: 2D plot of the difference between the TA Spectrum of pure CdTe nanocrystals (Fig. S15) and CdTe@CdSe/CdS nanorods (Fig. S8). In both measurements the sample was pumped at a central Wavelength of 640 nm. To account for slight differences in concentration the TA Signal from the CdTe nanocrystals was scaled by a factor of 0.8, which minimised the coherence artefact.

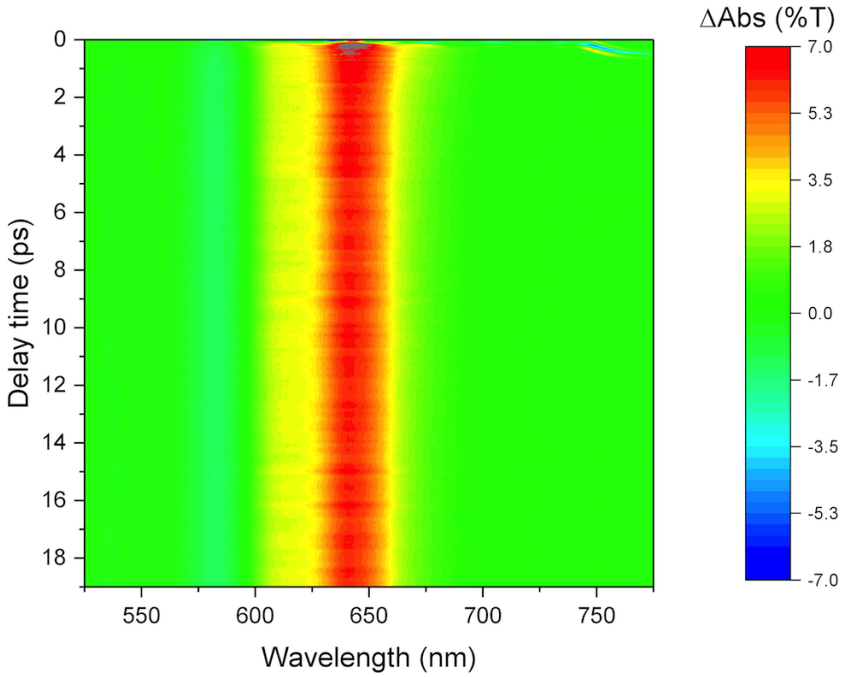

Figure S17: 2D plot of the chirped TA spectrum of pure CdTe nanocrystals with a diameter of 4.5 nm after treatment with $CdCl_2$. The sample was pumped at 640 nm.

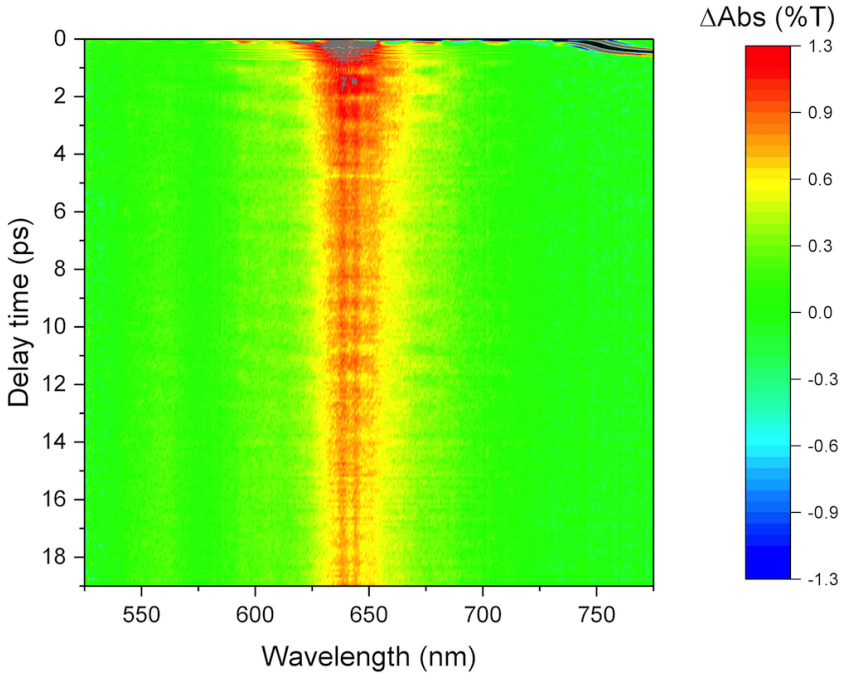

Figure S18: 2D plot of the chirped TA spectrum of CdTe@CdSe/CdS nanorods with a 2.9 nm CdSe seed after treatment with $CdCl_2$. The sample was pumped at 640 nm. Scattering artifacts are caused by an excess of $CdCl_2$.

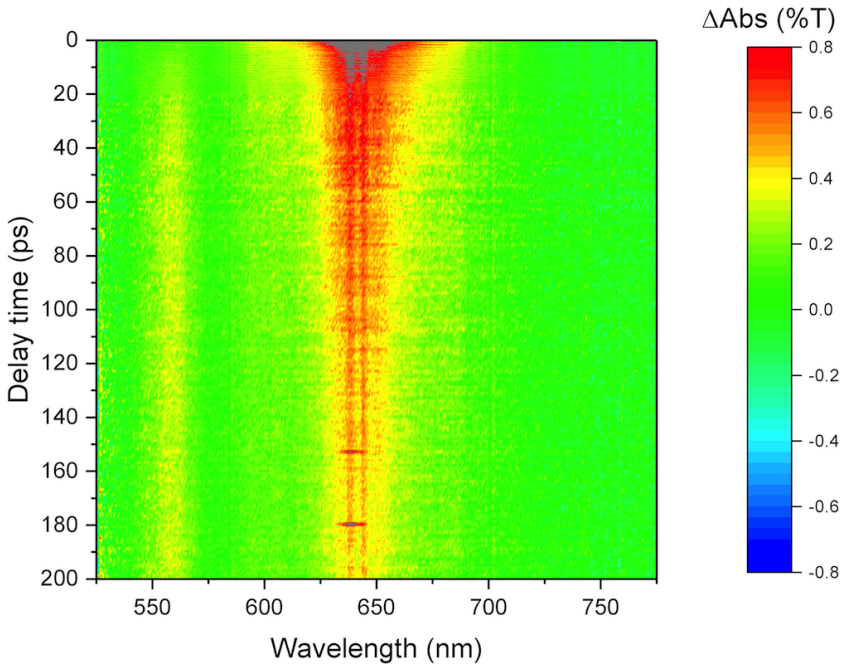

Figure S19: Same data as in Figure S18, but showing the full temporal window of the experiment (200 ps) with adjusted color map. The gray regions are due to high signal due to scattering from the sample.

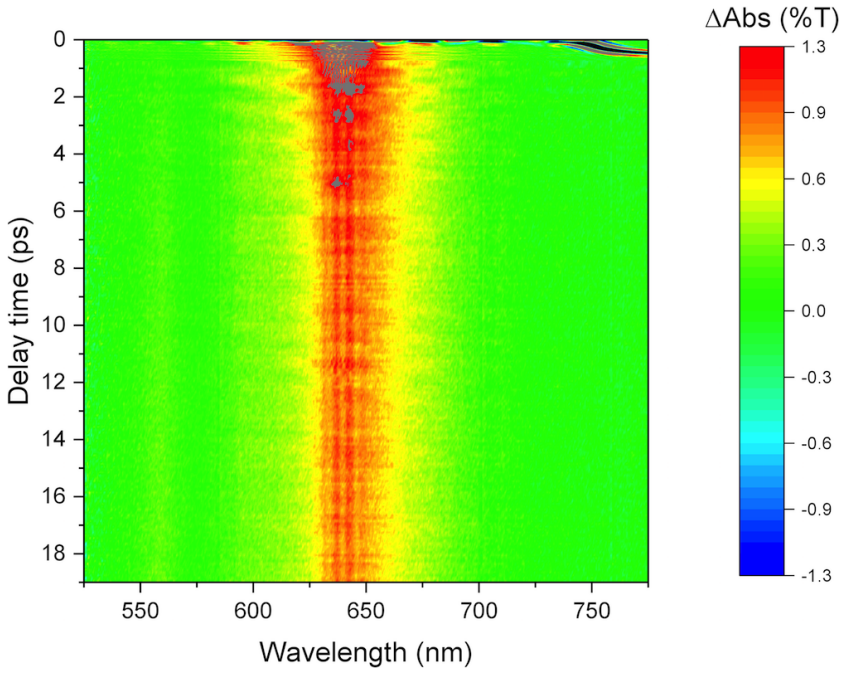

Figure S20: 2D plot of the chirped TA spectrum of CdTe@CdSe/CdS nanorods with a 2.9 nm CdSe seed after treatment with $CdCl_2$ and in the presence of 4-MPA. The sample was pumped at 640 nm.

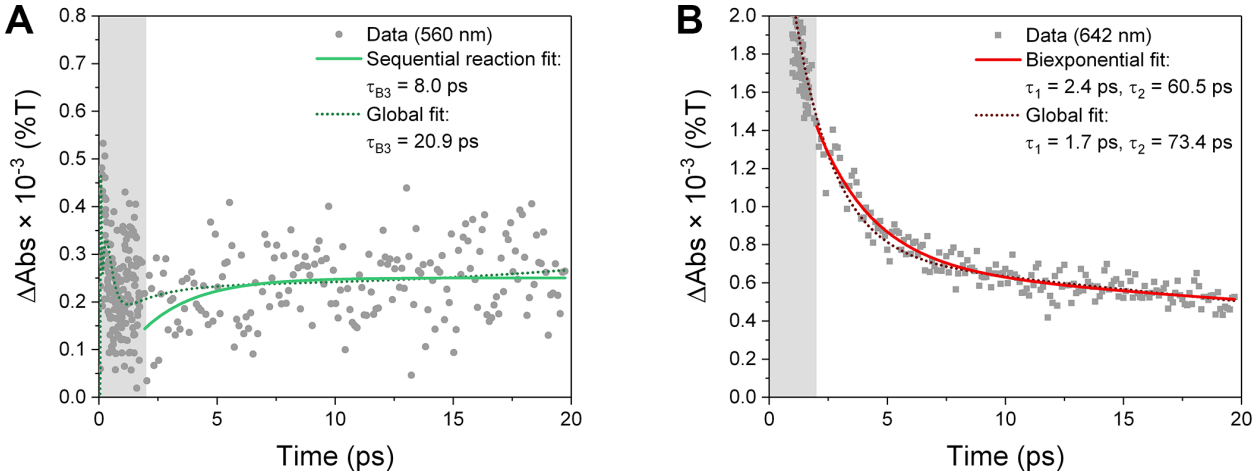

Figure S21: Decay of the CdTe@CdSe/CdS nanorods with 2.9 nm seeds at 560 nm (A) and 642 nm (B) after pumping at 640 nm. No hole scavenger was added and single wavelength and global fits are shown. The maximal amplitude for the trace at 560 nm is $A_{B3} = 1.1 \times 10^{-4}$, the total amplitude for the trace at 642 nm is $A_1 + A_2 = 2.4 \times 10^{-3}$, which amounts to a < 5 % transfer efficiency. The relatively large discrepancy between the global and local fits for τ_{B3} is explained by the low S/N of the data and the resulting large error. The discussion in the main text is based on the global fit parameters.

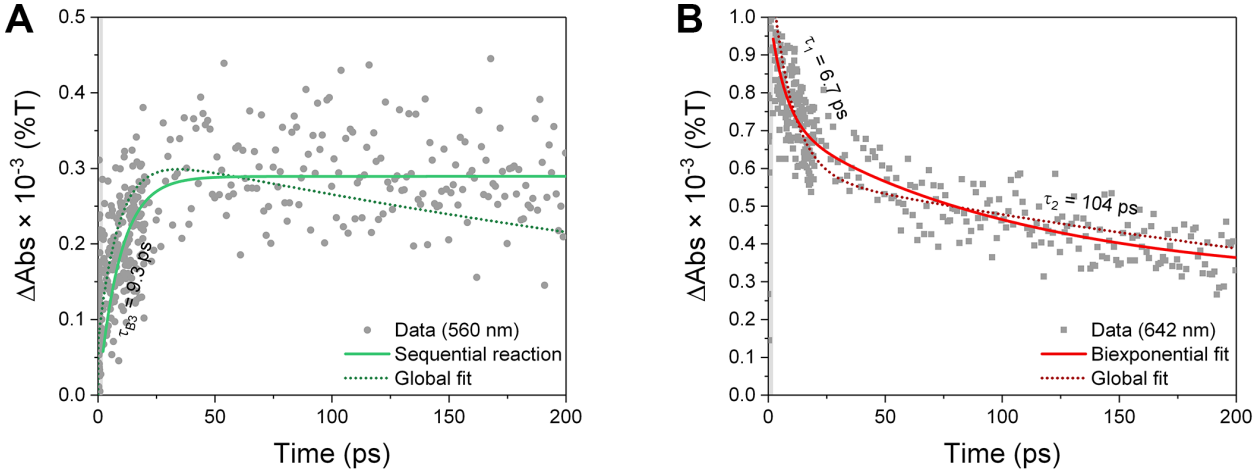

Figure S22: Decay of the CdTe@CdSe/CdS nanorods after treatment with $CdCl_2$ at 560 nm (A) and 642 nm (B), pumped at 640 nm. No hole scavenger was added and single line and global fits are shown. The maximal amplitude for the trace at 560 nm is $A_{B3} = 2.9 \times 10^{-4}$, the total amplitude for the trace at 642 nm is $A_1 + A_2 = 7.3 \times 10^{-4}$, which amounts to a 40 % transfer efficiency. The global fit visibly deviates from the data at 560 nm. Note the different scaling of the time axis compared to Figure S21. (The same data is shown in Figure 6B of the main text.)

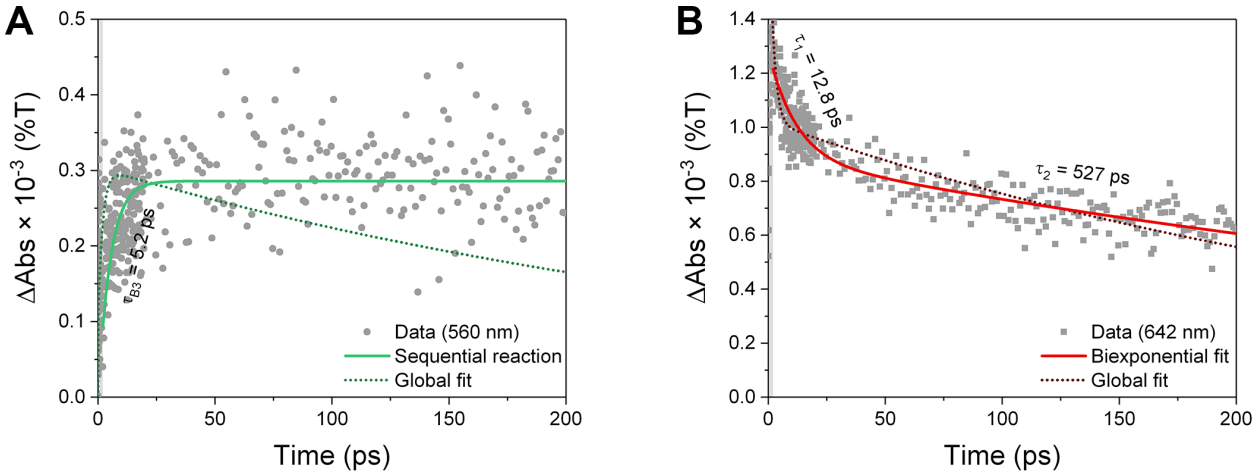

Figure S23: Decay of the CdTe@/CdSe/CdS nanorods after treatment with $CdCl_2$ and in the presence of 4-mercaptophenol at 560 nm (A) and 642 nm (B), pumped at 640 nm. Single line and global fits are shown. The maximal amplitude for the trace at 560 nm is $A_{B3} = 2.9 \times 10^{-4}$, the total amplitude for the trace at 642 nm is $A_1 + A_2 = 12.5 \times 10^{-4}$, which amounts to a 23 % transfer efficiency. The global fit visibly deviates from the data at 560 nm. The lack of hole scavenging efficiency is attributed to the passivated and saturated nanorod surface.

Geometry used for the EMA calculations

The EMA calculations were performed on a geometric model based on the hexagonal shape of a typical CdS nanorod: The CdSe seed was modelled as a sphere with a diameter taken from TEM data (2.9 or 4.0 nm) and placed 2/3 of the length of the rod away from the CdTe tip. For the CdS nanorod a 15 nm long, hexagonal prism was used. Its radius was set 0.3 nm thicker than the seed to account for a fully embedded seed, as per TEM data. At the tip at which the CdTe was grown a hexagonal pyramid with a height of 1.45 nm was added to model the shape of the faster growing end of the nanorod. The CdTe tip was composed of two hexagonal pyramids and a hexagonal prism with a total length of $(1.45 + 3.0 + 1.45)$ nm and the same cross section as the CdS nanorod. This seed was offset from the CdS tip by a variable distance and placed either centred with respect to the axis of the nanorod or shifted to better model the real shape of the particles. A rectangular grid with a resolution of 0.2 nm was used for all calculations.

Use of other hole scavengers than 4-mercaptophenol

Of other hole scavengers that were tested phenothiazine showed a weaker effect ($\sim$ 35 % with respect to 4-MPH),[3] while lithium triethylborohydride,[4] ferrocene, and ferrocenecarboxylic acid showed no significant increase of B3 at 560 nm.

References

1. Adachi, S. *Properties of Group-IV, III-V and II-VI Semiconductors*, 1st ed.; Wiley Series in Materials for Electronic and Optoelectronic Applications; John Wiley & Sons, Ltd: Chichester, 2005.

2. Wei, S.-H.; Zunger, A. Calculated Natural Band Offsets of all II–VI and III–V Semiconductors: Chemical Trends and the Role of Cation *d* Orbitals. *Appl. Phys. Lett.* **1998**, *72*, 2011.

3. Wu, K.; Du, Y.; Tang, H.; Chen, Z.; Lian, T. Efficient Extraction of Trapped Holes from Colloidal CdS Nanorods. *J. Am. Chem. Soc.* **2015**, *137*, 10224–10230.

4. Rinehart, J. D.; Schimpf, A. M.; Weaver, A. L.; Cohn, A. W.; Gamelin, D. R. Photochemical Electronic Doping of Colloidal CdSe Nanocrystals. *J. Am. Chem. Soc.* **2013**, *135*, 18782–18785.